CHEMISTRY
A EUROPEAN JOURNAL

FULL PAPER

DOI: 10.1002/chem.201204105

Nucleation and Growth of Chrysotile Nanotubes in $H_2SiO_3/MgCl_2/NaOH$ Medium at 90 to 300 °C

Romain Lafay,*[a] German Montes-Hernandez,*[a] Emilie Janots,[a] Rodica Chiriac,[b] Nathaniel Findling,[a] and François Toche[b]

Abstract: Herein, we report new insights into the nucleation and growth processes of chrysotile nanotubes by using batch and semi-continuous experiments. For the synthesis of this highly carcinogenic material, the influences of temperature (90, 200, and 300 °C), Si/Mg molar ratio, and reaction time were investigated. From the semi-continuous experiments (i.e., sampling of the reacting suspension over time) and solid-state characterization of the collected samples by XRPD, TGA, FTIR spectroscopy, and FESEM, three main reaction steps were identified for chrysotile nucleation and growth at 300 °C: 1) formation of the proto-serpentine precursor within the first 2 h of the reaction, accompanied by the formation of brucite and residual silica gel; 2) spontaneous nucleation and growth of chrysotile between about 3 and 8 h reaction time, through a progressive dissolution of the proto-serpentine, brucite, and residual silica gel; and 3) Ostwald ripening growth of chrysotile from 8 to 30 h reaction time, as attested to by BET and FESEM measurements. Complementary results from batch experiments confirmed a significant influence of the reaction temperature on the kinetics of chrysotile formation. However, FESEM observations revealed some formation of chrysotile nanotubes at low temperatures (90 °C) after 14 days of reaction. Finally, doubling the Si/Mg molar ratio promoted the precipitation of pure smectite (stevensite-type) under the same P (8.2 MPa)/T (300 °C)/pH (13.5) conditions.

Keywords: chrysotile · growth factors · nanotubes · solvent effects · thermogravimetric analysis

Introduction

Serpentine is a widespread mineral that results from hydrothermal alteration of the oceanic lithosphere.[1] Various serpentine polymorphs, such as antigorite, lizardite, chrysotile, and polygonal serpentine, have been observed in natural systems.[2] Chrysotile is the most common fibrous serpentine (Mg3Si2O5(OH)4). Preliminary studies on chrysotile have shown a significant curvature of the unit cell compared to conventional crystal structures.[3] Chrysotile fibrils are composed of layers that are either curved concentrically or spirally with fivefold symmetry[4] into a nanometric tubular structure (22–27 nm)[5] around either the x axis (clinochrysotile[6] and orthochrysotile[7]) or around the y axis (parachrysotile[8]). The hollow cores of the nanotubes have a diameter of about 5–8 nm.[9] The association between chrysotile and polygonal serpentine has also been addressed[10] and, in natural systems, proto-serpentine has been recognized as a potential chrysotile precursor[11,12] during the early dissolution/precipitation reactions in the alteration of the oceanic lithosphere. However, this so-called proto-serpentine precursor has rarely been observed in experimental systems.[12] One recent study reported that glass alteration under hydrothermal conditions was dominated by the formation of proto-chrysotile, which does not have the fully well-defined crystallinity and cylindrical shape like chrysotile.[13] Natural chrysotile minerals are highly heterogeneous and typically correspond to an assembly of different chrysotile polytypes and/or serpentine polymorphs than can contain abundant trace elements or mineral inclusions.[14–16] These heterogeneities account for the variety of chrysotile morphologies that are observed in nature (e.g., cylindrical, tube-in-tube, or conical)[17] and the multitude of serpentine assemblies.

Chrysotile syntheses have been investigated for several decade.[17,18] The health hazards of this asbestos, especially the carcinogenicity, is known.[19] Recently, scientists/engineers have developed innovative routes to obtain nanosized-to-submicrometric chrysotile particles of various shapes and sizes.[20–23] For this purpose, the most popular reported reactants are MCM41 (specific surface area: about 900 $m^2 g^{-1}$) or enstatite ($MgSiO_3$) as a Si source[24–26] and synthetic brucite, MgO periclase, or $MgCl_2$ soluble salt as a Mg source.[27] Most of the previous studies were performed in a moveable vessel with a volume of around 500 cm^3 under stirring, but

[a] R. Lafay, Dr. G. Montes-Hernandez, Dr. E. Janots, N. Findling
Institut des Sciences de la Terre (ISTerre)
UJF-CNRS, 38041, Grenoble, Cedex 9 (France)
Fax: (+33) 476-635-252
E-mail: romain.lafay@ujf-grenoble.fr
german.montes-hernandez@ujf-grenoble.fr

[b] Dr. R. Chiriac, F. Toche
Laboratoire des Multimatériaux et Interfaces
UMR CNRS 5615, 43 bd du 11 novembre 1918
69622 Villeurbanne Cedex (France)

they generally used pre-treated reactants. Typically, all of these reported chrysotile syntheses were performed in alkaline medium (NaOH) to promote the incorporation of $-OH$ ions. The influence of several parameters, such as temperature,[20,28] pH value,[28] and Mg substitution (e.g., Ni and Fe),[29–36] and the role of trace elements (e.g., Li)[37] have also been investigated. Most of the experimental studies synthesized chrysotile at a temperature of 300 °C and some of these studies revealed an optimal temperature of between 300 and 400 °C.[21–23,31,35] The longest chrysotile nanotubes reported so far were obtained at 400 °C after a reaction time of 168 h. Conversely, the reaction kinetic and crystallinity of chrysotile decrease at temperatures <300 °C.[28] However, very few studies have focused on the nucleation and growth processes of chrysotile because batch (or discontinuous) reactors are generally used.[22,23,29]

In some studies, the transformation from proto-serpentine into chrysotile has been interpreted as the curvature of nanoflakes beyond a certain threshold, thus resulting in the formation of nanotubes through a solid-state-transition process.[28] In 2012, Bloise et al. suggested that the experimental conditions played a major role in determining the stability of the proto-chrysotile.[13] Conversely, our semi-continuous experiments (i.e., sampling of the reacting suspension over time) suggested the dissolution of the proto-serpentine precursor, followed by the precipitation of chrysotile (this study). This controversial interpretation has direct implications on the presence/absence/role of a pre-nucleation process during the hydrothermal or solvothermal formation of a given mineral or bio-mineral, which is a current "hot topic" in science.[38]

This study has a twofold objective: Firstly, to determine the reaction steps and kinetics of chrysotile formation from a H_2SiO_3/$MgCl_2$/NaOH slurry by using batch and semi-continuous experiments and, secondly, to determine the influence of reaction temperature and Si/Mg molar ratio on chrysotile formation. We have developed an innovative route for chrysotile formation by directly using commercial silica gel (H_2SiO_3; i.e., without pre-treatment) instead of MCM41 as a Si source. Solid-state experimental products were characterized by using X-ray powder diffraction (XRPD), Fourier-transform IR spectroscopy (FTIR), field-emission gun scanning electron microscopy (FESEM), N_2-adsorption isotherms, and thermogravimetric analysis (TGA/SDTA). This latter analytical tool was particularly efficient to accurately determine the abundance of chrysotile and brucite as a function of time.

Experimental Section

Reactants: Silica gel material H_2SiO_3 was purchased from Strem Chemicals in 99% chemical purity and high specific surface area ($830\ m^2\ g^{-1}$); however, additional N_2-adsorption isotherm measurements revealed a lower specific surface area ($600\ m^2\ g^{-1}$) and XRPD diffraction confirmed the dominant amorphous material. Magnesium chloride hexahydrate ($MgCl_2{\cdot}6H_2O$) and sodium hydroxide (NaOH) were purchased from ROTH in ≥ 99% chemical purity. Reactants were used with no preliminary treatment.

Batch experiments: A 1 M solution of NaOH (250 mL), silica gel (H_2SiO_3, 1.302 g), and magnesium chloride hexahydrate ($MgCl_2{\cdot}6H_2O$, 5.082 g) were placed in a Parr copper-alloy reactor (autoclave with an internal volume of 0.5 L). This aqueous reaction system was immediately stirred under constant mechanical agitation (300 rpm) during the reaction. Then, the aqueous system was heated at 300 °C for 30 h by using a heating jacket that was fitted to the reactor, followed by preliminary experiments on chrysotile syntheses. To evaluate the influence of temperature on the synthesis, three supplementary experiments were performed, at 90 °C for 14 and 30 days and at 200 °C for 2 days. Finally, the influence of the Si/Mg molar ratio (from 1 to 1.33) was evaluated by modifying only the initial amount of silica gel in the system. These latter experiments were performed at 300 °C for 30 h.

At the end of the experiment, the autoclave was removed from the heating system and immersed in cold water. After cooling in water at 30 °C (for about 15 min), the autoclave was disassembled and the solid product was carefully recovered and separated by centrifugation (20 min at 11500 rpm), with decantation of the supernatant solutions. The solid product was washed twice through re-dispersion/centrifugation processes to remove any soluble compounds (e.g., NaCl and Na_2CO_3) that were co-formed during the synthesis and subsequent quenching. Finally, the solid product was dried directly in the centrifugation flasks at 90 °C for 48 h. The dry solid product was manually recovered, weighed, and stored in plastic flasks for further characterization (FESEM, XRPD, TGA, N_2-adsorption isotherms, and FTIR spectroscopy).

Semi-continuous experiments: The semi-continuous system (sampling with time) was operated under optimized conditions (300 °C, Si/Mg = 0.67) to monitor the composition of the solid product in the samples ex situ. About 10 mL of the dispersion was sampled in the reactor as a function of time during the nucleation and growth of chrysotile. Two experiments were performed: The dispersion was collected after 1, 2, 3, 4, 6, and 8 h and after 12, 16, 20, and 30 h in the two semi-continuous experiments, respectively. For the two experiments, the collected dispersion was cooled by water circulation in the sampling system. The solid-product-recovery/drying procedures were similar to those described above for the batch experiments.

The experimental conditions and mineral composition of the solid products from all of the syntheses are summarized in Table 1.

Solid-state characterization

X-ray powder diffraction (XRPD): All samples were manually crushed before analysis. Powders were carefully placed and manually compacted in borosilicate capillaries (diameter: 500 μm), which corresponded to about 5 mg of sample. XRPD patterns were recorded on a Bruker D8 powder diffractometer that was equipped with a SolX Si (Li) solid-state detector from Baltic Scientific Instruments by using $Cu_{K\alpha1\text{-}K\alpha2}$ radiation and a Göbel mirror. Intensities were recorded from 5 to 80° with an 8 s counting time per 0.024° 2θ step for the of determination bulk mineralogy. For experiments that contained clays, complementary oriented thin sections were prepared and treated in an atmosphere of ethylene glycol to determine the change in interlayer space by XRPD measurements.

Field-emission gun scanning electron microscopy (FESEM): The reaction products were characterized by using secondary or backscattered electrons. Microimaging was performed on a Zeiss Ultra 55 FESEM with a spatial resolution of approximately 1 nm at 15 kV. The samples were dispersed in absolute EtOH by ultrasonic treatment for at least 5 min to deaggregate the particles. One or two drops of the dispersion were placed onto an aluminum support and coated with a thin film of Pt for the SEM observations.

Differential thermal analysis and thermogravimetric analysis (DTA/TGA): Experimental solid products were characterized on a TGA/SDTA 851e

Table 1. Summary of the experimental conditions and mineral composition of the products.[a]

Run	t [h]	T [°C]	Si [mol L^{-1}]	Mg [mol L^{-1}]	Si/Mg molar ratio	Products	pH value	TGA mass loss [%]	
								Serpentine	Brucite
1	1	300	0.067	0.1	0.67	P-S≫B	13.3	5.90	9.54
2	2	300	0.067	0.1	0.67	P-S≫B	13.38	5.45	8.64
3	3	300	0.067	0.1	0.67	Ctl+P-S≫B	13.38	11.84	6.01
4	4	300	0.067	0.1	0.67	Ctl≫B	13.46	8.05	3.43
5	6	300	0.067	0.1	0.67	Ctl≫B	13.39	10.57	2.52
6	8	300	0.067	0.1	0.67	Ctl	13.4	10.90	–
7	12	300	0.067	0.1	0.67	Ctl	13.39	10.03	–
8	16	300	0.067	0.1	0.67	Ctl	13.38	10.53	–
9	20	300	0.067	0.1	0.67	Ctl	13.39	10.91	–
10	30	300	0.067	0.1	0.67	Ctl	13.39	12.02	–
12	48	200	0.067	0.1	0.67	P-S≫Ctl≫B	13.4	6.90	7.94
13	336	90	0.067	0.1	0.67	B≫P-S≫Ctl	13.35	n.d.	15.14
14	720	90	0.067	0.1	0.67	B≫P-S≫Ctl	13.38	n.d.	13.62
15	30	300	0.133	0.1	1.33	Sm	13.45	n.d.	n.d.
16	30	300	0.1	0.1	1	Ctl≫Sm≫B	13.38	n.d.	n.d.

[a] All of the experiments were performed on unreacted starting material at pH≈13.5 (measured at 25°C at the beginning and end of the experiments). The saturated pressures were 8.2, 1.6, and 0.1 MPa at temperatures of 300, 200, and 90°C, respectively. B = brucite, Ctl = chrysotile, P-S = proto-serpentine, Sm = smectite, n.d. = not determined.

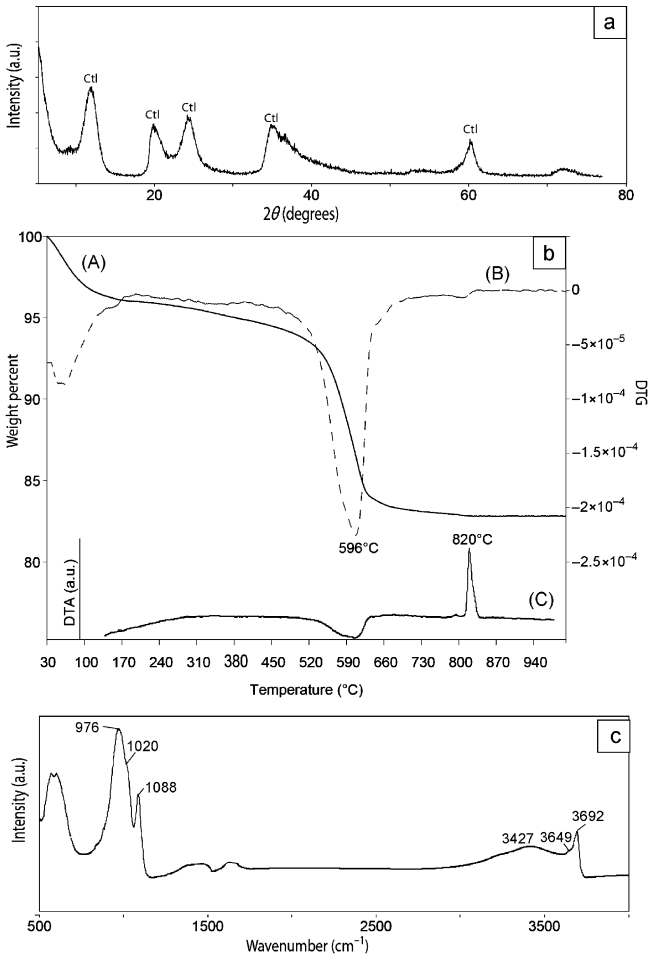

Figure 1. Characterization of synthetized chrysotile after 30 h reaction time (Run 10): a) Experimental XRPD pattern, Ctl = chrysotile; b) TG first derivative (DTG, B), and the corresponding DTA spectra (C); c) FTIR spectrum..

Mettler Toledo instrument under the following conditions: Sample mass: about 10 mg, platinum crucible (150 μL) with a pinhole, heating rate: 10°C min^{-1}, inert N_2 atmosphere: 50 mL min^{-1}. The mass loss in the sample and the associated thermal effects were determined by TGA/DTA in the temperature range 30–1200°C. To identify the different mass-loss steps, the first derivatives of the TGA data (rate of mass loss) were used. The TGA apparatus was calibrated in terms of mass and temperature; calcium oxalate was used to calibrate the sample mass and the melting points of three compounds (indium, aluminum, and copper) that were obtained from the DTA signals were used to calibrate the sample temperature. The temperature accuracy of the TGA/SDTA system was about ±0.25°C. The weighting accuracy was about 0.1 μg, which corresponded to 0.01% for a 10 mg sample. The losses of mass that were associated to the brucite and serpentine phases, as deduced by TGA, are summarized in Table 1.

Fourier-transform IR spectroscopy (FTIR): Measurements (in transmission mode) were performed on a Bruker Hyperion 3000 IR microscope. The IR beam was focused through a ×15 lens and the typical size of the IR aperture was 50×50 μm^2. The light source was a Globar(TM) and the beam splitter was in KBr. The spectra were measured from 700 to 4000 cm^{-1} (resolution: 4 cm^{-1}) with a MCT monodetector that was cooled by liquid nitrogen.

Samples were prepared with respect to a flat thickness of <100 μm. Sample preparation involved careful sample crushing in a mortar and manual compaction of the finely crushed particles between two KBr windows. Five spectra per sample were recorded and OPUS software was used to fit the results and to compare the spectra from the experimental products.

N_2-sorption isotherms: N_2-sorption isotherms for Runs 6, 10, 12, 14, and 15 were performed on a Micrometrics ASAP 2010 system. The specific surface areas of the powdered samples were estimated by applying the Brunauer–Emmett–Teller (BET) equation in the relative-pressure range $0.05 < P/P_0 < 0.35$ and by using the cross-sectional area of molecular N_2 (16.2 Å^2). In addition, the Barrett, Joyner, and Halenda (BJH) method, which take into account capillary condensation by using the Kelvin equation, was used for the determination of the pore-size distribution.

Results and Discussion

A detailed characterization of the textural properties (size, morphology, specific surface area) of chrysotile that was synthesized under the optimized conditions (T = 300°C, Si/Mg = 0.67), the reaction steps during the crystal-growth process, and the influence of temperature and Si/Mg molar ratio on the synthesis are given below. Herein, we report new insights into the nucleation and growth processes of chrysotile nanotubes by using semi-continuous experiments.

Textural properties and purity of chrysotile: Figure 1 shows the solid-state characterization (XRPD, TGA, FTIR spec-

troscopy) of chrysotile that was precipitated under optimized conditions, that is, 300 °C (water-saturation pressure: about 80 bar) for 30 h with a stoichiometric molar ratio of Si to Mg with respect to the structural formula of serpentine (Table 1, Run 10).

The experimental XRPD pattern is characterized by broad peaks and it successfully matches with International Centre for Diffraction Data (ICDD) card #27-1275, which corresponds to the chrysotile mineral (Figure 1 a). The broad peaks indirectly indicate the presence of very small particles/crystallites, as confirmed by FESEM observations (Figure 2).

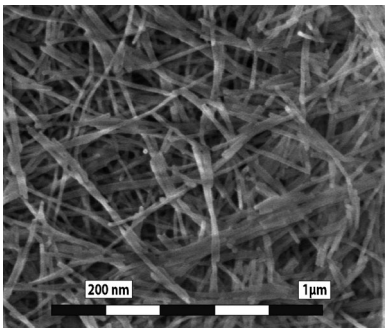

Figure 2. FESEM image showing the synthesis of chrysotile after 30 h at 300 °C (Run 10).

Herein, the typical length of the chrysotile nanotubes is about 450 nm, for a width of about 16 nm, based on an average analysis of 200 particles. Moreover, TGA indicates one single dehydroxylation event, which corresponds to a global loss of mass that is close to 11 %, peaking at 596 °C (Figure 1 b and Table 1).

This loss of mass involves a broad endothermic peak at about 600 °C and a sharp exothermic peak at 820 °C in the DTA pattern (Figure 1 b), thus indicating the crystallization of the remaining amorphous anhydrous material (the so-called meta-chrysotile $Mg_3Si_2O_7$) into forsterite (Mg_2SiO_4).

This result is in agreement with literature reports.[39] Finally, the FTIR spectrum (Figure 1 c) shows stretching bands for the hydroxy group at 3692 cm^{-1}. The band for the Si–O group in chrysotile is characterized by three specific peaks (976, 1020, and 1088 cm^{-1}).[40] The two less-intense peaks, at 1450 and 1640 cm^{-1}, indicate the presence of a carbonate stretching band and a bending vibration of molecular water, respectively.

Complementary N_2-sorption isotherms revealed a high specific surface area (S_{BET} = 185 $m^2 g^{-1}$, Figure 3). The two branches of the hysteresis loop converge at P/P_0 = 0.6. This result indicates a wide distribution of pore sizes, as already seen in synthetic chrysotile.[41] The BJH pore-size distribution was in the range 2–70 nm, with a median that was equivalent to 21.5 nm, which was indicative of a mesoporous material. The corresponding cumulative pore volume (0.64 $cm^3 g^{-1}$) is higher than the values reported in the literature for synthetic chrysotile.[38,39]

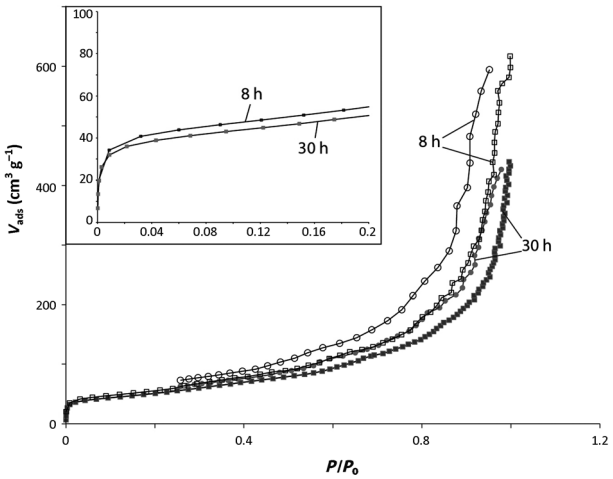

Figure 3. N_2-adsorption/desorption isotherms of synthetic chrysotile after 8 h (Run 6) and 30 h reaction time (Run 10). Inset: the range $0 < P/P_0 < 0.2$.

Reaction steps and kinetics of chrysotile precipitation: At 350 °C under water-saturation pressure, Korytkova et al.[29] determined by using XRPD that chrysotile spontaneously co-precipitated with brucite between 2 and 3 h reaction time and that, after about 6 h reaction time, only chrysotile was observed. Jancar and Suvorov[28] proposed that the formation of chrysotile nanotubes resulted from the curvature of the nanoflakes serpentine precursor beyond a certain threshold size, that is, through a solid-state transition. In 2012, Bloise et al. suggested that proto-chrysotile and chrysotile could co-exist in experimental systems.[13] Conversely, our semi-continuous experiments suggest dissolution of the proto-serpentine precursor, followed by the precipitation of chrysotile, as explained below.

The mechanism for the precipitation of chrysotile from a H_2SiO_3/$MgCl_2$/NaOH slurry at 300 °C can be summarized in three main sequential reaction steps: 1) formation of the proto-serpentine precursor and brucite within the first 2 h reaction time; 2) spontaneous nucleation and growth of chrysotile between about 3 and 8 h reaction time, through the progressive dissolution of proto-serpentine, brucite, and residual silica gel; and 3) Ostwald ripening growth of chrysotile from 8 to 30 h reaction time.

Formation of proto-serpentine precursor: The broad features in the XRPD pattern after 2 h reaction time indicate the formation of a poorly crystallized material (Figure 4 a). This result is attributed to the formation of proto-serpentine, as supported by the flake-like morphology observed by FESEM (Figure 5 a) and TGA (Figure 6). DTG curves after 1 and 2 h reaction time show a broad feature between 450 and 650 °C, which can be interpreted as the dehydroxylation of proto-serpentine and corresponds to a loss of mass of about 5.5–5.9 %. Well-crystallized brucite was also formed within this time (Figure 5 a) and the DTG curve showed a single peak close to 400 °C. In agreement with the XRPD

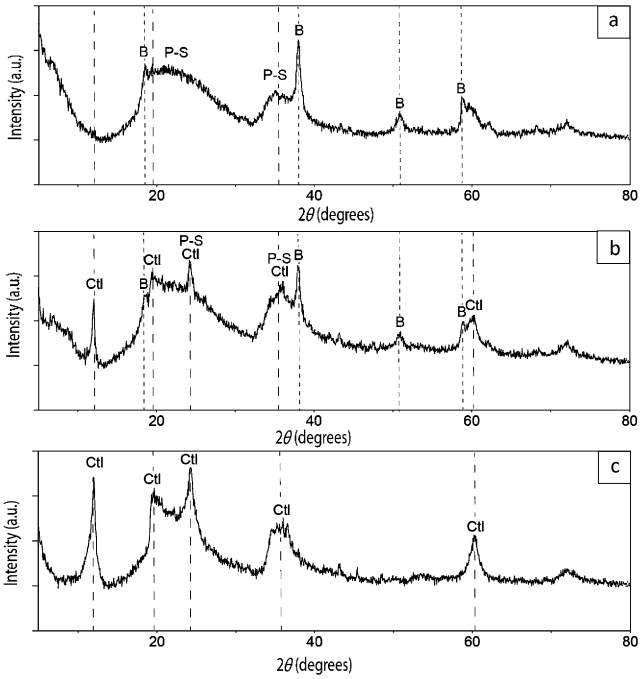

Figure 4. Experimental XRPD patterns for chrysotile at 300 °C after: a) 2 h (Run 2), b) 3 h (Run 3), and c) 8 h reaction time (Run 6). B = brucite (X-ray ICDD card #74-2220), P-S = proto-serpentine, Ctl = chrysotile.

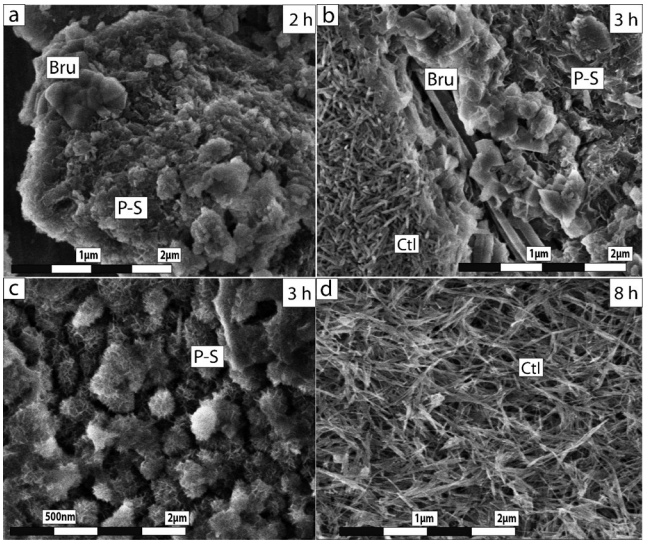

Figure 5. FESEM images for samples that were collected after: a) 2 h (Run 2), b) 3 h (Run 3), c) 3 h (magnified image of the proto-serpentine), and d) 8 h reaction time (Run 6, pure chrysotile nanotube). Bru = brucite, P-S = proto-serpentine, Ctl = chrysotile.

data, this peak was attributed to the dehydroxylation of brucite mineral. The similarity between the mass losses after 1 and 2 h reaction time (about 9 %) indicates an apparent sta-

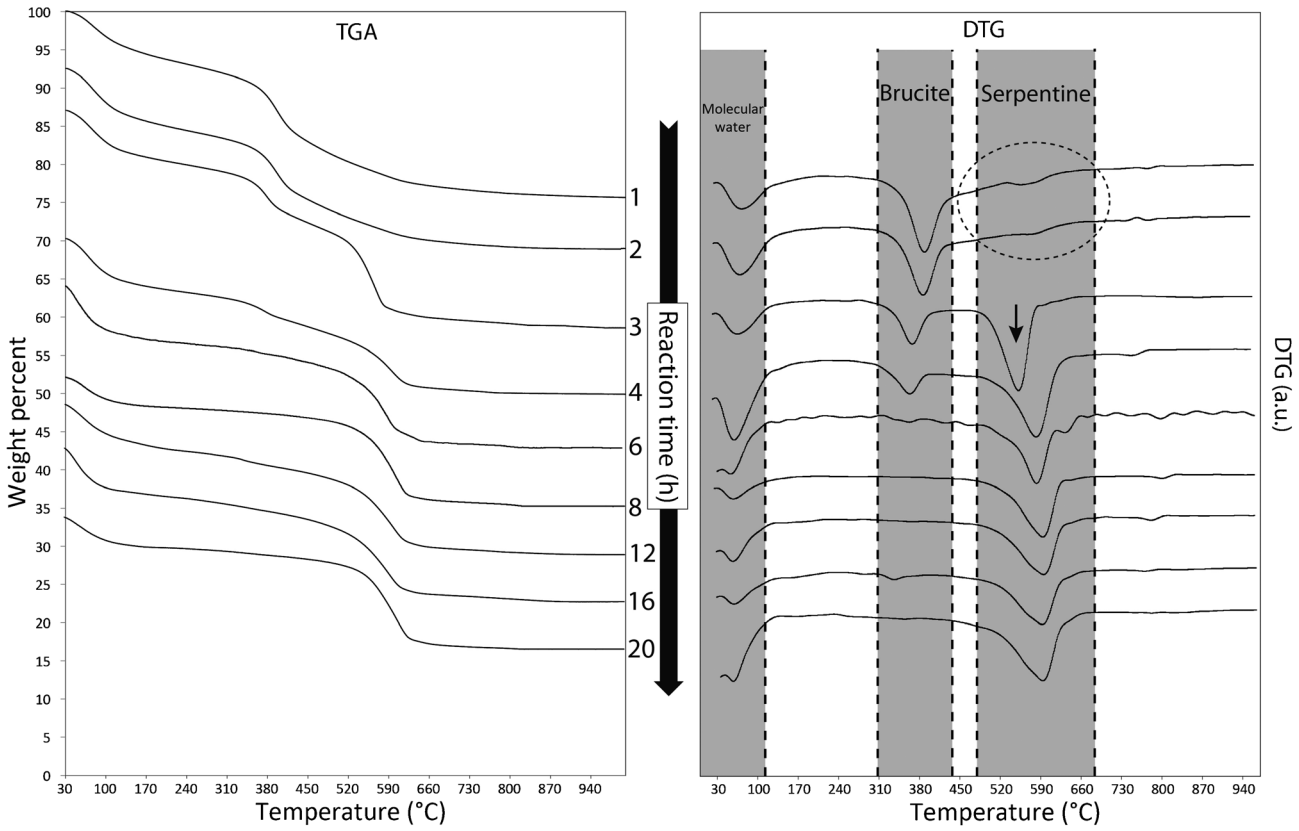

Figure 6. TG measurements and the corresponding first-derivate curves (DTG) of samples that were collected during the nucleation and growth of chrysotile. Dotted ellipsoids indicate the proto-serpentine dehydroxylation range; arrow indicates chrysotile-nucleation event after 3 h reaction time.

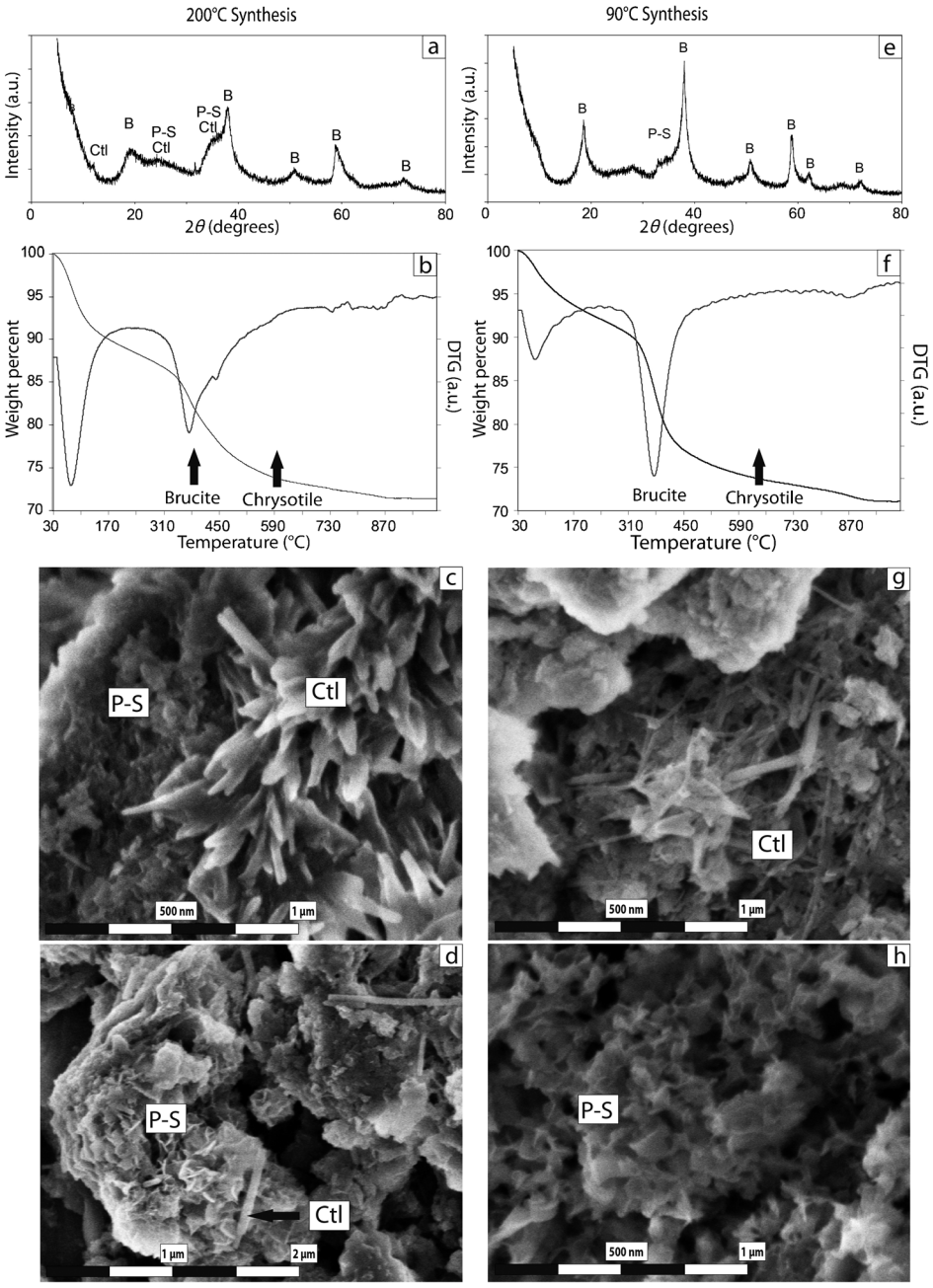

Figure 7. Influence of reaction temperature on chrysotile formation at 200 °C (a–d, Run 12) and 90 °C (e–h, Run 14). a,e) Experimental XRPD patterns, b,f) TG curves, c–h) FESEM images. B = brucite, Ctl = chrysotile. The positions of the DTG peaks for reference chrysotile and brucite that were synthetized at 300 °C (Run 10) are reported for comparison.

bilization during this period. In summary, we have provided clear evidence for the formation of proto-serpentine with a nanometric flake-like morphology within the first 2 h of the reaction, accompanied by fast precipitation of brucite.

Nucleation and growth of chrysotile: The experimental XRPD pattern of the solid product after 3 h reaction time reveals the formation of chrysotile (ICDD card #27-1275), which co-exists with the so-called proto-serpentine and brucite (Figure 4b). The presence of proto-serpentine induces persistent broad features that overlap the chrysotile peaks. FESEM observations confirm the presence of chrysotile nanotubes (length: 260 nm, width: 17 nm, average of 50 particles) that are well-dispersed in proto-serpentine and micrometric brucite assemblies (Figure 5b,c). TG measurements show the typical dehydroxylation peak for serpentine, but shifted to lower temperatures compared to the batch experiments (shift from 600 to 555 °C). No exothermic peak was identified at 820 °C (Figure 1b), probably owing to small particle size and/or low amount of chrysotile mixed with residual proto-serpentine (Figure 6). Conversely, a typical dehydroxylation-temperature peak was observed close to 600 °C, with its associated exothermic peak after 4 h reaction time.

The X-ray diffraction peaks that correspond to brucite decrease significantly in intensity between 3 and 4 h reaction time. This result is in agreement with the TG measurements, in which the brucite content decreases progressively and no brucite is detected after 8 h (Figure 4c and Figure 6). Proto-serpentine is still observed after 3 h reaction time, but FESEM observations indicate that it completely disappears within 4 h. Single chrysotile was detected/observed by XRPD, TGA, and FESEM after 8 h reaction time; the TGA measurements indicate strong variations in the content of the serpentine phase between 3 and 8 h reaction time (Table 1).

Based on these results, we assume that the crystal growth process of chrysotile proceeds through the simultaneous dissolution of proto-serpentine and brucite. In our system, the identified proto-serpentine could play two important roles: firstly, it could act as a nucleation agent for chrysotile and, secondly, it could provide the required chemical elements for chrysotile growth. As mentioned above, this process is in disagreement with a solid-state-transition process previously suggested by Jancar and Suvorov.[28]

Ostwald ripening growth of chrysotile: As discussed above, only the chrysotile mineral was detected and/or observed after 8 h reaction time (Figure 4c, Figure 5d, and Figure 6), that is, an apparent equilibrium was reached between chrysotile and the interacting solution after this reaction time in the system. However, when different particle-size populations co-exist in a given interacting fluid, Ostwald ripening growth can be active and it is often promoted at high temperatures. Thus, conventional BET measurements revealed that the specific surface area decreased from 206 $m^2 g^{-1}$ (8 h reaction time) to 185 $m^2 g^{-1}$ (30 h, Figure 3). Based on this result and some FESEM observations, we concluded that the Ostwald ripening growth particularly took place between 8 and 30 h at 300 °C, that is, the smaller chrysotile crystals dissolved and the dissolved species were re-deposited on the surfaces of larger chrysotile crystals.

Influence of the temperature: In agreement with literature reports,[20,28] the reaction temperature plays a crucial role in determining the formation kinetics of chrysotile. For example, Figure 7 summarizes the XRPD, TGA, and FESEM results at two different reaction temperatures (90 and 200 °C). Herein, chrysotile particles with tubular morphology were observed by FESEM at both temperatures. However, no clear evidence for the formation of chrysotile was obtained in the XRPD and TGA measurements on the solid-state products, possibly owing to its low proportion after the investigated reaction time of 2 days at 200 °C or after 14 and 30 days at 90 °C. Only brucite was clearly identified as the crystalline phase in both cases. In analogy with the reaction steps that were deduced from semi-continuous experiments (see above), we suspect that we reach the chrysotile nucleation event at 200 °C after 2 days reaction time. The evidence for chrysotile-nucleation events at lower temperatures (90 °C) after 14 and 30 days reaction time is less convincing. In summary, the reaction temperature has a strong influence on the formation kinetics of chrysotile, but it could also have a significant effect on the reaction pathway (e.g., the inhibition of chrysotile formation and the stabilization of other silicate phases).

On the other hand, N_2-sorption isotherms revealed a high specific surface area, that is, $S_{BET}=133.5\ m^2 g^{-1}$ after 2 days at 200 °C and $S_{BET}=233$ and $125.62\ m^2 g^{-1}$ after 14 and 30 days at 90 °C, respectively. The adsorption and desorption branches present a large hysteresis (Figure 8) and do not completely close until the relative pressure in the desorption branch returns to $P/P_0=0.4$, thus indicating a microporous material. This result was confirmed by applying the BJH method on the sorption isotherms. Herein, the pore size is lower than 8 nm, with a median at around 3.8 nm, for both syntheses (Figure 8, insets). The cumulative pore volume was 0.32 $cm^3 g^{-1}$ after 30 days at 90 °C and 0.20 $cm^3 g^{-1}$ after 2 days at 200 °C.

Influence of the Si/Mg ratio: As described above, pure chrysotile was obtained at 300 °C after 30 h reaction time by using a Si/Mg molar ratio of about 0.67, which corresponded to the Si/Mg ratio in the serpentine mineral ($Mg_3Si_2O_5(OH)_4$). The initial amount of the Si and Mg sources and the Si/Mg molar ratio significantly influenced the purity of chrysotile. Higher Si concentrations (Si/Mg > 0.70) systematically induced the precipitation of a swelling clay with a stevensite (Mg smectite) structural formula $(Na)_x(Mg)_{3-x}(Si_4O_{10})(OH)_2{\cdot}nH_2O$. This smectite co-precipitated with chrysotile and brucite. Mg smectite was found to be the sole mineral phase when the Si/Mg ratio was constrained to 1.33. The N_2-sorption isotherm revealed a moderate specific surface area, $S_{BET}=83.75\ m^2 g^{-1}$, and the conventional "ethylene glycol test" confirmed the swelling properties of this synthesized material (Figure 9). FESEM analysis (Figure 9, inset) shows a cornflake-like morphology, which is typical of smectite clay.

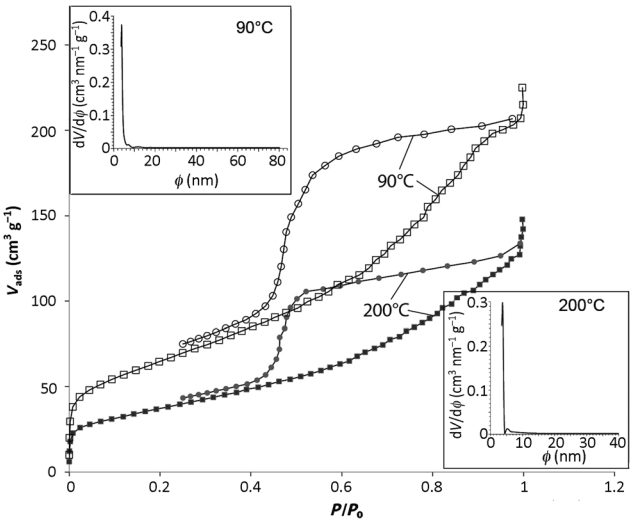

Figure 8. N_2-adsorption/desorption isotherms of the synthesized products after 2 days at 200 °C (Run 12) and 14 days at 90 °C (Run 13).

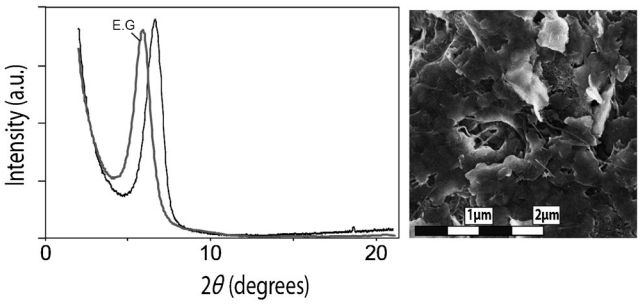

Figure 9. Experimental XRPD patterns for an experiment at 300 °C with Si/Mg = 1.33 (Run 14) before and after treatment with ethylene glycol (E.G.) and the corresponding FESEM image.

Conclusion

We showed that chrysotile synthesis at 300 °C is the result of a complex reaction pathway. Proto-serpentine and brucite

appear as transient phases during the first step of the reaction (first 2 h). Then, chrysotile is spontaneously nucleated from suspension and growth through the simultaneous dissolution of proto-serpentine and brucite from 3 to 8 h reaction time. The last step of the reaction is characterized by Ostwald ripening growth of chrysotile from 8 to 30 h reaction time. Complementary experiments confirmed a strong influence of the reaction temperature on the kinetic formation of chrysotile. For example, chrysotile can be formed at 90 °C, but only some particles of chrysotile were observed after 14 days reaction time. Finally, variation of the Si/Mg molar ratio constrained the mineral composition in the final product under same *P*/*T*/pH conditions.

Acknowledgements

The authors are grateful to the French National Center for Scientific Research (CNRS) and the University Joseph Fourier (UJF) in Grenoble for financial support. R.L. was supported by a PhD grant from the French Education Ministry.The authors are grateful to O. Vidal, who allowed the use of a sophisticated autoclave to perform various experiments.

[1] J. B. Moody, *Lithos* **1976**, *9*, 125–138.
[2] C. Mével, *Comptes Rendus Geosciences* **2003**, *335*, 825–852.
[3] E. J. W. Whittaker, *Acta Crystallogr.* **1955**, *8*, 571–574.
[4] G. Cressey, B. A. Cressey, F. J. Wicks, K. Yada, *Mineralogical Magazine* **2010**, *74*, 29–37.
[5] K. Yada, *Acta Crystallogr. Sect. A* **1971**, *27*, 659–664.
[6] E. Whittaker, *Acta Crystallogr.* **1956**, *9*, 855–862.
[7] E. Whittaker, *Acta Crystallogr.* **1956**, *9*, 862–864.
[8] E. Whittaker, *Acta Crystallogr.* **1956**, *9*, 865–867.
[9] B. A. Cressey, E. J. W. Whittaker, *Mineralogical Magazine* **1993**, *57*, 729–732.
[10] A. Baronnet, B. Devouard, *Can. Mineral.* **2005**, *43*, 513–542.
[11] M. Andreani, A. Baronnet, A.-M. Boullier, J.-P. Gratier, *Eur. J. Mineral.* **2004**, *16*, 585–595.
[12] M. Andreani, O. Grauby, A. Baronnet, M. Muñoz, *Eur. J. Mineral.* **2008**, *20*, 159–171.
[13] A. Bloise, E. Belluso, M. catalano, E. Barrese, D. Miriello, C. Apollaro, *J. Am. Ceram. Soc.* **2012**, *95*, 3050–3055.
[14] D. R. Veblen, P. R. Buseck, *Science* **1979**, *206*, 1398–1400.
[15] D. S. O'Hanley, J. V. Chernosky, F. J. Wicks, *Can. Mineral.* **1989**, *27*, 483–493.
[16] F. J. Wicks, D. S. O'Hanley, *Rev. Mineral. Geochem.* **1988**, *19*, 91–167.
[17] K. Yada, K. Iishi, *Am. Miner.* **1977**, *62*, 958–965.
[18] K. Yada, K. Iishi, *J. Cryst. Growth* **1974**, *24–25*, 627–630.
[19] E. Foresti, E. Fornero, I. G. Lesci, C. Rinaudo, T. Zuccheri, N. Roveri, *J. Hazard. Mater.* **2009**, *167*, 1070–1079.
[20] E. Korytkova, A. Brovkin, T. Maslennikova, L. Pivovarova, I. Drozdova, *Glass Phys. Chem.* **2011**, *37*, 161–171.
[21] E. N. Korytkova, A. V. Maslov, L. N. Pivovarova, Y. V. Polegotchenkova, V. F. Povinich, V. V. Gusarov, *Inorg. Mater.* **2005**, *41*, 743–749.
[22] G. Falini, E. Foresti, M. Gazzano, A. F. Gualtieri, M. Leoni, I. G. Lesci, N. Roveri, *Chem. Eur. J.* **2004**, *10*, 3043–3049.
[23] G. Falini, E. Foresti, G. Lesci, N. Roveri, *Chem. Commun.* **2002**, 1512–1513.
[24] C.-F. Cheng, W. Zhou, D. Ho Park, J. Klinowski, M. Hargreaves, L. F. Gladden, *J. Chem. Soc. Faraday Trans.* **1997**, *93*, 359–363.
[25] Q. Cai, W.-Y. Lin, F.-S. Xiao, W.-Q. Pang, X.-H. Chen, B.-S. Zou, *Microporous Mesoporous Mater.* **1999**, *32*, 1–15.
[26] M. Grün, I. Lauer, K. K. Unger, *Adv. Mater.* **1997**, *9*, 254–257.
[27] E. N. Korytkova, A. V. Maslov, L. N. Pivovarova, I. A. Drozdova, V. V. Gusarov, *Glass Phys. Chem.* **2004**, *30*, 51–55.
[28] B. Jancar, D. Suvorov, "*The Influence of Hydrothermal-Reaction Parameters on the Formation of Chrysotile Nanotubes*," can be found under http://iopscience.iop.org/0957-4484/17/1/005, **2006**.
[29] E. Korytkova, L. Pivovarova, V. Gusarov, *Geochem. Int.* **2007**, *45*, 825–831.
[30] E. Korytkova, L. Pivovarova, I. Drosdova, V. Gusarov, *Russian Journal of General Chemistry* **2007**, *77*, 1669–1676.
[31] E. Korytkova, L. Pivovarova, *Glass Phys. Chem.* **2010**, *36*, 53–60.
[32] A. Bloise, E. Belluso, E. Barrese, D. Miriello, C. Apollaro, *Cryst. Res. Technol.* **2009**, *44*, 590–596.
[33] A. Bloise, E. Belluso, E. Fornero, C. Rinaudo, E. Barrese, S. Capella, *Microporous Mesoporous Mater.* **2010**, *132*, 239–245.
[34] A. Bloise, E. Barresse, C. Apollaro, *Neues Jahrb. Mineral. Abh.* **2009**, *185*, 297–304.
[35] E. Foresti, M. F. Hochella, H. Kornishi, I. G. Lesci, A. S. Madden, N. Roveri, H. Xu, *Adv. Funct. Mater.* **2005**, *15*, 1009–1016.
[36] F. Turci, M. Tomatis, I. G. Lesci, N. Roveri, B. Fubini, *Chem. Eur. J.* **2011**, *17*, 350–358.
[37] B. Wunder, F. Deschamps, A. Watenphul, S. Guillot, A. Meixner, R. Romer, R. Wirth, *Contrib. Mineral. Petrol.* **2010**, *159*, 781–790.
[38] D. Gebauer, A. Völkel, H. Cölfen, *Science* **2008**, *322*, 1819–1822.
[39] A. Cattaneo, F. Gualtieri, G. Artioli, *Phys. Chem. Miner.* **2003**, *30*, 177–183.
[40] G. Anbalagan, G. Sivakumar, A. R. Prabakaran, S. Gunasekaran, *Vib. Spectrosc.* **2010**, *52*, 122–127.
[41] A. McDonald, B. Scott, G. Villemure, *Microporous Mesoporous Mater.* **2009**, *120*, 263–266.

Received: November 16, 2012
Published online: February 27, 2013

